Optics & Laser Technology 181 (2025) 111626

Contents lists available at ScienceDirect

Optics and Laser Technology

journal homepage: www.elsevier.com/locate/optlastec

Full length article

An investigation into the use of incoherent UV light to augment IR nanosecond pulsed laser texturing of CFRP composites for improved adhesion

Ahmed Al-Mahdy *, Juan Ignacio Ahuir-Torres, Tahsin T Öpöz, Hiren R Kotadia, Jack Mullett, Martin C Sharp

General Engineering Research Institute, School of Engineering, Faculty of Engineering and Technology, Liverpool John Moores University, Byrom Street, Liverpool L3 3AF, United Kingdom

ARTICLE INFO

Keywords:
Infrared laser
Ultraviolet light
Surface treatment
Laser texturing
CFRP composites
Adhesive bonding

ABSTRACT

The preparation of Carbon Fibre Reinforced Polymers (CFRP) surfaces for adhesive bonding has been widely reported. Such reports include laser texturing using both near-infrared (IR) lasers and ultraviolet (UV) lasers. In this report, we present, for the first time, findings showing that surface treatment of CFRP using incoherent UV light, at 254 nm wavelength, can increase the adhesive bonding strength of CFRP by 75 % compared to non-treated samples. It is also around 10 % stronger than NIR laser-textured samples. However, combination treatments, where the UV irradiation is conducted either before or after laser texturing did not give a significant benefit over the laser-textured samples. A germicidal 46 W 254 nm UV lamp was used for the UV light treatment, while an IR nanosecond pulsed fibre laser operating at 1064 nm was used for the laser texturing treatment. The material tested was an autoclave-cured T700 CFRP composite.

The wettability of the treated CFRP surfaces and the adhesive bonding were quantitatively assessed. This study concludes that low-cost incoherent UV treatment effectively reduces the water contact angle of the CFRP surface and activates CFRP surfaces. All treatments led to bonding strengths at least 50% greater than for the untreated surfaces.

The predominant failure mode for UV-treated samples was Cohesive Substrate Failure (CSF), indicating that the adhesion strength exceeded the interlaminar shear strength of the CFRP material. All samples treated with the laser (including combined treatment with UV) exhibited Light Fibre Tear Failure.

1. Introduction

CFRP composites are being used across industries such as aerospace, wind energy, automotive, oil and gas extraction, and sports equipment. They reduce weight and offer high rigidity, as well as excellent static and fatigue strength compared to metals [1,2]. Moreover, the increasing demands to reduce fuel consumption and minimise carbon emissions encourage aircraft manufacturers (e.g., Airbus (A380), Boeing (787)) and automobile (e.g., BMW) manufacturers to use CFRP and other light composites in the fabrication of their product structures. Manufacturing of CFRP structures is a complicated process, often created with joining several elements together [2]. Mechanical joints, such as rivets, are widely used. These have several drawbacks; the abrasive and anisotropic properties of CFRPs lead to high tool wear and greater cutting forces while drilling and a harmful effect on the workpiece integrity. Delamination, cracks, and matrix thermal degradation are observed as a result of uncontrolled tools [3]. Adhesive bonding avoids the above drawbacks and gives a good compromise of fatigue strength and stiffness. Moreover, adhesive joints are cost and weight-efficient [2]. However, strong, and durable adhesive joints are not straightforward to create. For a given adhesive and joint design, the main factors governing adhesive joint strength are the conditions of the surfaces to be bonded together, their roughness, wettability, and cleanliness [4]. The surface roughness increases the actual bonded interface area and adds mechanical

Abbreviations: AF, Adhesive Failure; CA, Contact Angle; CF, Carbon Fibre; CFRP, Carbon Fibre Reinforced Polymer; CSF, Cohesive Substrate Failure; IR, Infrared; LFTF, Light Fibre Tear Failure; SEM, Scanning Electron Microscopy; SLS, Single Lap Shear; UD, Unidirectional; UV, Ultraviolet; WCA, Water Contact Angle.

* Corresponding author.
E-mail address: a.k.almahdy@2020.ljmu.ac.uk (A. Al-Mahdy).

https://doi.org/10.1016/j.optlastec.2024.111626
Received 19 March 2024; Received in revised form 6 June 2024; Accepted 12 August 2024
Available online 20 August 2024
0030-3992/© 2024 The Authors. Published by Elsevier Ltd. This is an open access article under the CC BY license (http://creativecommons.org/licenses/by/4.0/).

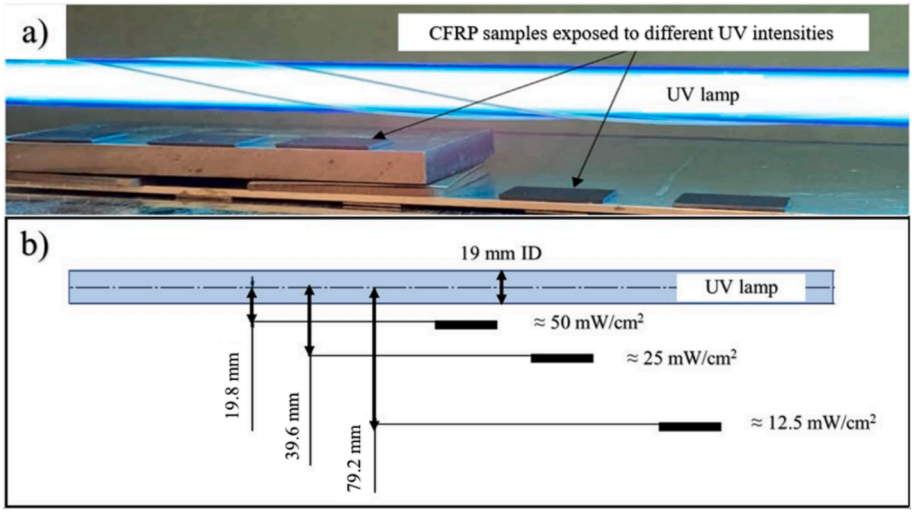

Fig. 1. UV lamp and the experimental setup: a) photograph and b) Schematic drawing.

interlocking between the substrate and the cured adhesive [5]. The consequence of good wetting is a greater contact area between the adherents and the adhesive over which the forces of adhesion may act. Contaminants, such as dirt, oil, moisture, release agents and weak layers, must be removed, otherwise, the adhesive will bond to these weak boundaries rather than to the substrate [6]. Therefore, surface preparation, prior to adhesive joining, to achieve clean and activated CFRP surfaces is crucial to ensure stronger joints [1,2].

Currently, different methods of surface preparation are employed, each with its own advantages and disadvantages. Mechanical treatments (sanding and sandblasting) are easily applicable but lead to damage to the carbon fibres (CFs) at the surface, have low reproducibility, and produce dust at the surface [7]. Peel ply is utilised to counter the drawbacks of typical mechanical surface preparation methods and generate uniform surface roughness. However, this approach introduces contaminants which can have a detrimental effect on bonding characteristics [8–10]. For over a decade, researchers have investigated different lasers to improve the surface adhesivity of CFRPs [2]. The benefits of employing lasers include their non-contact nature, resulting in the absence of cutting forces. There are no concerns regarding tool wear, and lasers can be integrated with robotic automation systems to achieve high processing speed [11]. Ultraviolet (UV) and infrared (IR) laser surface texturing generally showed enhancement in joint strength with encouraging results using UV lasers [12]. UV laser treatment is considered a cold process that directly breaks down molecular bonds by photoablation. However, it has limited reliability, high power consumption, and a high cost of ownership [13]. IR lasers on the other hand, which are the most widely used laser source in industry, process materials by intense local heating that melts or vaporises part of the material surface. This can cause damage to the surrounding areas or affect the fibre–matrix integrity [12].

Several researchers have investigated non-laser UV light treatments, to improve polymeric or non-polymeric material surfaces for adhesive bonding [14–20]. These studies were mostly based on using UV light accompanied with ozone, by either applying ozone or using UV sources that emit at a wavelength less than 240 nm producing ozone in the surrounding atmosphere. Studies have reported UV/ozone treatment proving effective in enhancing joint strength across various materials, surpassing methods like grit blasting and primers. However, UV/ozone treatment requires special facilities with high corrosion resistance to ozone, which may be impractical, especially for larger structures. Moreover, ozone is highly toxic [21].

UV light can influence polymer surfaces in two different ways; first, it directly photo-degrades and/or photo-crosslinks the polymer molecular bonds. The second effect, associated with wavelength lower than 240 nm, is indirect and results from the interaction of the UV light with atmospheric oxygen creating ozone, atomic oxygen, and oxygen radicals that oxidise and modify the polymer surface [22,23]. In general, photodegradation of polymers occurs in the μm or sub-μm order of depth from the surface, with the highest effect closest to the surface, where an accumulated layer of the degraded species is believed to absorb UV irradiation more strongly and reduce the penetration of UV light into the inner part of polymers [24].

This study aims to investigate the effect of UV light radiation emitted by a germicidal lamp at 254 nm on improving the adhesive bonding of CFRP surfaces and compare the results of this technique with IR fibre laser texturing, either used solely or in combination with UV treatment. Exposing CFRP surfaces to a certain UV fluence was found to be a viable and cost-effective alternative to other techniques for improving adhesive bonding. To the best of the author's knowledge, no similar research has been published.

2. Experimental

2.1. Materials

CFRP laminates with a thickness of 1.43 ± 0.02 mm were fabricated at Reverie Ltd. (UK) using an autoclave. The laminates consisted of five layers of Unidirectional (UD) prepreg (*SHD MTC510-UD300-T700-33–35 % 300 mm wide*) laid up at alternating angles of (0°/90°/0°/90°/0°). According to its datasheet, the prepreg material is manufactured using T700 CFs and has a tensile strength and modulus of 2300 MPa and 119 GPa, respectively, in the direction of the fibres, and its interlaminar shear strength is 84 MPa. For the CFRP panels, in-house destructive tensile tests were performed that showed an average tensile strength of 1500 MPa parallel to the direction of the CFs at the surface. This means for a 25 mm wide sample, a load of about 56 kN is needed for failure, which is 5–6 times the anticipated adhesive failure loads.

For surface treatments and adhesive joining investigations, the CFRP panels were cut using a water-cooled cut-off saw *(Erbauer 750 W)* with a diamond cutting blade. The produced samples were immediately cleaned with de-ionized water and then in an ultrasonic bath of isopropanol. Moreover, a cross-section study performed on different (non-treated, treated, and failed after adhesively joined) CFRP samples has shown that for the non-treated material, the distance from surface to the embedded fibres is ranged between 10–20 μm, (see section 2.7). Araldite 420, a two components room curing epoxy adhesive was used to join the coupons for the Single Lap Shear (SLS) test procedure. According to the

Table 1
The uv lamp characteristics.

Parameter	Value
Power input (W)	130
UV output power (W)	46
Wavelength λ (nm)	254
Lamp length (mm)	740
Lamp diameter (mm)	19

Table 2
UV intensities and distances from the lamp applied in this study.

Distance from the lamp centre (mm)	UV intensity (mW/cm^2)
19.8	50
39.6	25
79.2	12.5

product datasheet, Araldite 420 achieves full strength, reaching 35 MPa at 22 °C, after 1 to 2 weeks of curing at room temperature.

2.2. UV equipment

A Germicidal UV lamp *(TUV Amalgam T6 130 W XPT SE G10.2q)* from Philips UK Ltd. was used in this study (Fig. 1a). Greater than 95 % of the light emitted is at 254 nm, Table 1 shows the lamp characteristics. The lamp illumination was assumed to be uniform and the UV intensity at a sample placed at a radius (r) away from the centre of the lamp was calculated by dividing the output power of the lamp by the cylindrical area (Table 2). The intensity of the light at a distance r from the axis of a long cylindrical source is inversely proportional to r [25].

The lamp was placed in a closed wooden box and to exclude any possible thermal effects, a cooling fan (0.55 m^3/min) was equipped to maintain near ambient conditions. A thermal infrared camera (*thermoIMAGER TIM)* from Micro-Epsilon UK was used to record the change in temperature over time at the surfaces of the samples. For the highest UV intensity (50 mW/cm2) applied in this experiment (Fig. 1b, Table 2), with the sample's top surface positioned approximately 10 mm away from the hot (85 °C) lamp, the temperature at the sample's surface increased initially and then stabilised after 10 min of exposure at 37 °C. This temperature was 14 °C higher than the room temperature. Moreover, a test to investigate whether there is a combined effect for the temperature on the Water Contact Angle (WCA) was done and there was no significant change in the measurements.

2.3. Laser equipment and parameters

The laser system used consisted of an infrared (IR) fibre laser, an optical system, and an automatic table with three axis (x,y,z). The laser model was a *SPI Laser (UK) G3 20 W* nanosecond pulsed fibre laser. The optical system consisted of a manually adjusted 1064 nm beam expander (*Linos (Qioptiq) 2-8x*), four silver mirrors (*Thorlab*), a galvanometric scanner (*Nutfield Extreme15-YAG*), and an f-theta lens of focal length (*f*) of 100 mm (*Linos Ronar F-Theta*). Fig. 2 illustrates a schematic drawing and photograph of this equipment and experimental setup.

The laser wavelength (λ) was 1064 ± 5 nm, with a beam quality factor $M^2 = 2.1$. The laser pulse length (τ) and repetition frequency (ν) were adjustable between 9 to 200 ns and 1 to 500 kHz respectively. The output beam is collimated to a diameter, D_0 approximately 5.7 mm (as measured by beam prints). The laser average power (P_{ave}) after the galvanometric scanner was measured with an *Ophir laser power meter system* and the pulse energy was calculated using Eq. (1) [26].

$$E_p = \frac{P_{ave}}{\nu} \tag{1}$$

The four mirrors guided the laser beam to the galvanometric scanner head that was fitted with a f-theta focussing lens. In this study, the displacement of the laser beam on the sample surface was handled by the galvanometric scanner, the three axis (x,y,z) table which held the sample was used to adjust the focal length. The theoretical laser beam diameter ($d_{o(Theo)}$) was around 51 μm, calculated using Eq. (2) [27,28].

Table 3
Selected laser parameters.

Parameter	Value
Pulse length, τ (ns)	200
Scan rate, v (mm/s)	850
Hatch space h (μm)	35
Theoretical focus beam size, $d_{(Theo)}$ (μm)	≈51
Pulse Repetition Frequency, ν (kHz)	25
Atmosphere	Air
Pulse Energy, E_p (μJ)	78
Pulse overlap (μm)	≈17
Hatch overlap (μm)	≈16
Pulse fluence (J/cm^2)	3.82

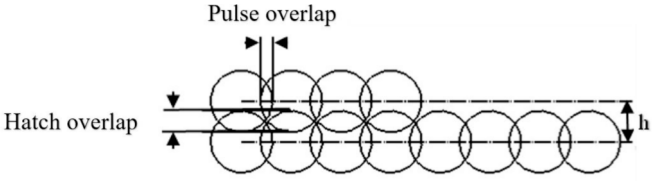

Fig. 3. Schematic for the laser scanning pattern.

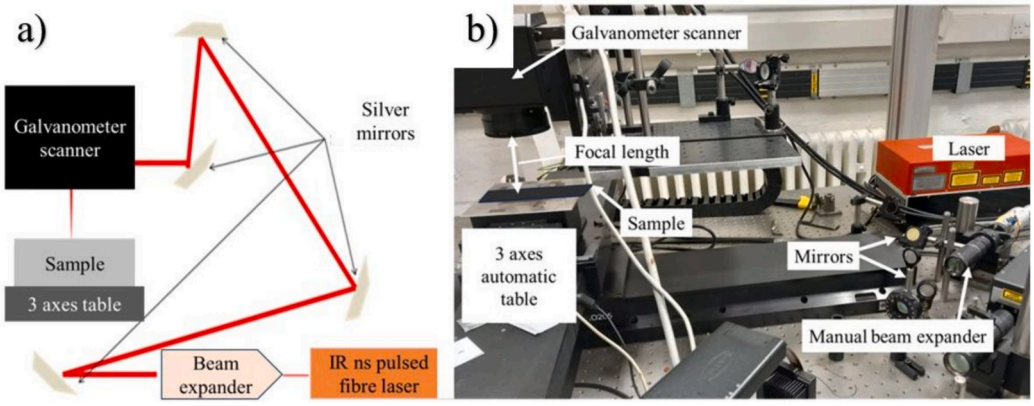

Fig. 2. Laser equipment and experimental setup: a) Schematic drawing and b) photograph.

Table 4
UV intensities and exposure periods adopted for WCA measurements.

UV intensity (mW/cm^2)	Exposure periods (min)					
12.5	15	30	45	60	90	120
25	15	30	45	60	90	120
50	15	30	45	60	90	120

Table 5
UV intensities and exposure periods adopted for bonding strength tests.

Treatment condition	Intensity (mW/cm^2)	Period (min)
UV1	50	60
UV2	25	120
UV3	50	120

Table 6
CFRP surface conditions adopted in the SLS tests.

Surface treatment condition						
Non-treated	UV1	UV2	UV3	IR	UV1 + IR	IR+UV1

$$d_{o(Theo)} = \frac{4f\lambda M^2}{\pi D_o} \quad (2)$$

The focussed laser beam was scanned at a scan rate (v) of 850 mm/s, uniaxial and perpendicular to the fibre orientation of the CFRP samples. The hatch spacing (h) between adjacent scans was 35 μm. The laser parameters (Table 3) and the scanning pattern (Fig. 3) for this study were selected following an optimisation study using a factorial experiment to ablate the outer layer matrix resin and expose the underlying CFs with minimum visual damage accompanied with the lowest WCA. The scanning involved only one overscan.

2.4. Wettability analysis

The wettability among the different surface treatment conditions has been assessed and compared by measuring the Water Contact Angle (WCA) using a goniometer and the sessile droplet method. A *CAM 101* from KSV Instruments Ltd (UK) was used to assess the surface wettability of the different treated samples. The diameter of the droplet out at the syringe was 1.5 mm. To capture the initial and the stable WCAs for the different UV-treated surfaces as well as the non-treated ones, 100 frames were recorded at a time interval of 16 ms and then 20 frames were recorded at a time interval of 1 s. For the laser-treated samples, due to the absorption behaviour of exposed fibres at the CFRP surfaces, a longer period (100 frames x 16 ms + 100 frames x 1 s) was used. For each surface condition, 15 repeated measurements were recorded, and the mean was calculated. All treated samples were cleaned twice using an ultrasonic bath of isopropanol once before the treatment and once before the CA assessment. Non-treated samples have only been cleaned prior to the WCA assessment.

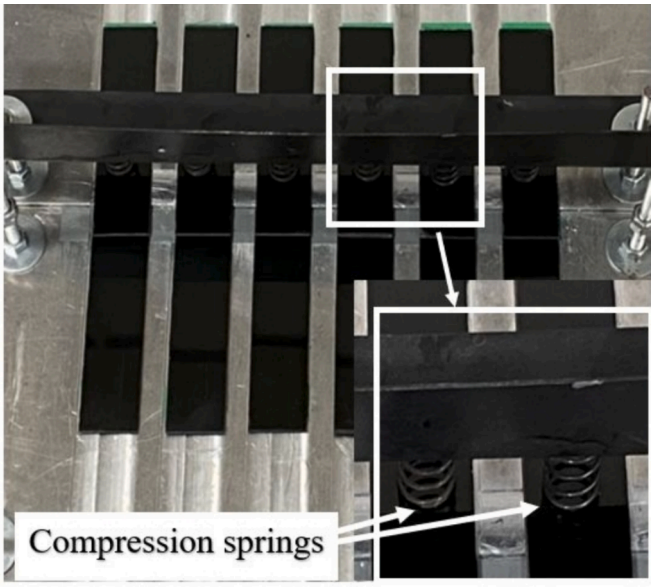

Fig. 5. Bonding jig capable of bonding six samples at a time, utilizes compression springs to ensure uniform adhesive thickness.

2.5. Design of experiment

The first part of this work was examining the effect of the UV exposure time with the different intensities on the reduction in WCA of CFRP surfaces. For each of the three different UV intensities, six CFRP samples, each 25 mm x 15 mm, were exposed for different periods (Table 4) starting from 15 min up to 120 min. The mean WCAs were then calculated based on 15 measurements immediately after the UV treatment.

The second part was comparing the bonding strength of CFRP coupons using Single Lap Shear (SLS) test among different surface conditions. For the UV treatment, three conditions were examined named as UV1, UV2, and UV3, (Table 5).

In addition to the UV treatment, IR laser texturing solely or combined (before or after) with UV treatments was implemented in the bonding strength comparison (Table 6). The purpose of the latter was to investigate the possible further enhancement to the bonding strength and to evaluate if the sequence of treatment has any impact.

2.6. Single Lap shear (SLS) tests

SLS tests were chosen to examine the adhesive bonding strength after the different surface treatments. BS EN ISO 1465:2009 [29], which is a commonly used standard for adhesive joining tests [7,12,30], was considered in this study. For symmetry and to minimise the eccentricity of the load path which causes out-of-plane bending moments, aluminium shims with the same thickness as the CFRP were adhesively bonded to the sample ends [31]. The sample dimensions are specified in Fig. 4.

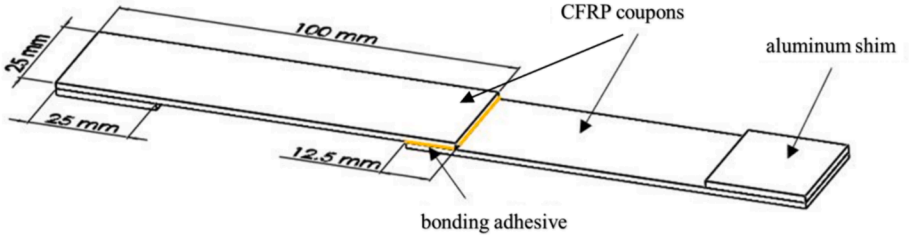

Fig. 4. Sample for SLS according to BS EN ISO 1465:2009 standard.

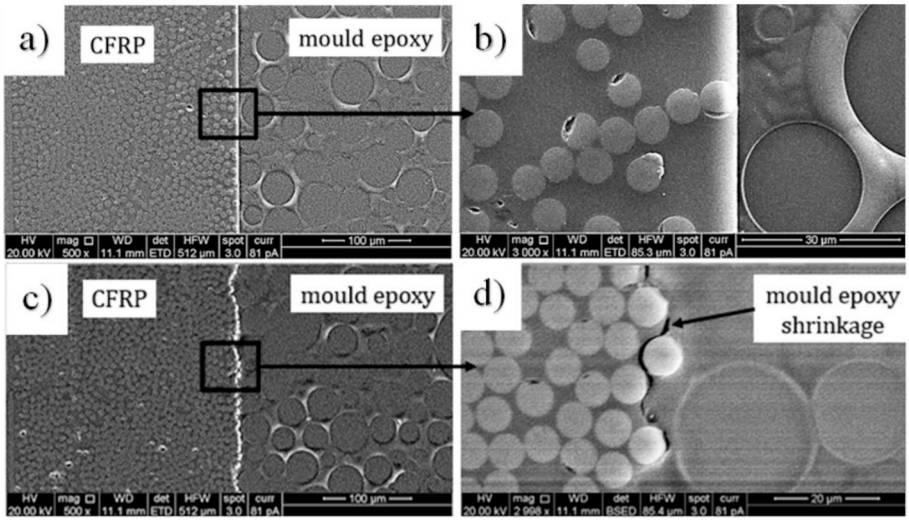

Fig. 6. SEM images of cross-section for CFRP material a) low magnification and b) high magnification for non-treated material, showing the distance from the surface to the CFs and the distribution of the CFs within the matrix resin, c) low magnification and d) high magnification of CFRP cross-section after laser texturing.

For each of the different surface conditions, six coupons were prepared in order to create three repeated couples to be tested. The prepared coupons were adhesively joined using a jig designed to join up to six couples at a time. The bondline thickness was 0.2 mm and was controlled using chopped pieces of copper wire (0.5 mm length x 0.2 mm diameter) that have been mixed with the adhesive before applying it to the lower coupons, glass beads have been similarly used in some previous studies [32]. The upper coupons were then applied, and steel compression springs, as shown in Fig. 5, each with a spring constant of 2.3 N/mm, were compressed 5 mm to produce a compression force of about 11.5 N, adequate to press the bonding adhesive layers uniformly over all the samples following the approach used by Bregar et al. [33]. The excess adhesive was then removed via a small spatula. The adhesive curing was performed at ambient conditions (20–23 °C) for 12 days. Afterwards, the samples were tested using a *Tinius Olsen 50 kN* tensile testing machine at a load rate of 1 mm/min.

2.7. Cross-section of the CFRP material

The distance from the outer surface of the CFRP coupon, through the outermost layer of resin to the surface of the carbon fibres were studied. Samples (15 mm x 15 mm) of non-treated CFRP material and laser textured were mounted vertically in an epoxy resin mould (*VersoCit-2*by Struers) then ground and polished. The grinding was conducted using paper grades of (80, 120, 240, 400, 600, 1200 and 2400) consecutively, in this process more than 1 mm of the samples was ground to dispose of the cut-effected edge. The polishing was conducted using three stages, two of them with diamond grit size 3 and 1 μm and the last was by using a solution (50/50 in volume) of distilled water and colloidal silica gel with a grain size of 40 nm. All polishing consumables were procured from Struers. Fracture analyses for the cross-section of the failed coupons after performing single lap shear tests was conducted using the same method described above. The polished cross-sections were then studied using optical microscopy and Scanning Electron Microscopy (SEM) (*Inspect S model*, Thermofisher) using both backscatter and secondary electron imaging with different magnifications.

3. Results and discussion

3.1. IR laser texturing

IR laser texturing had achieved the exposure of the carbon fibres at the surface. Fig. 6a and 6b show low and high magnification SEM images

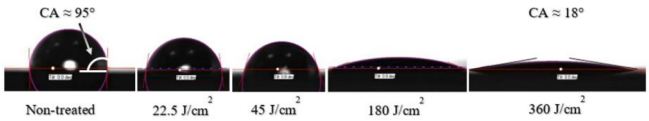

Fig. 7. Droplet shapes and the WCA at different UV fluence.

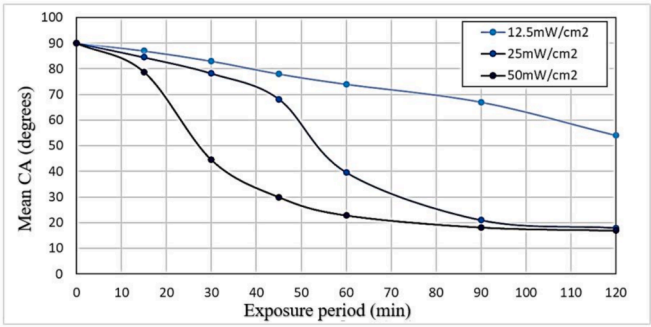

Fig. 8. Mean WCAs for CFRP samples treated with different UV intensities and exposure periods.

of the cross-section of a non-treated sample, the distance from the surface to the carbon fibres appeared to be as low as 1 μm in some positions, but mostly ranged between 10–20 μm. Fig. 6c and 6d show SEM images of the cross-section of a laser-textured sample. The carbon fibres at the surface are mostly exposed without visible damage. As the ablation mechanism of the outer layer matrix resin depends on the heating up of the underlying carbon fibres via the laser power transmitted through the resin, the bonding strength and integrity of the fibres at the surface with the matrix resin are possibly affected and weakened. The consequence of this weakening the integrity of the surface fibres is discussed in section 3.3.

3.2. Wettability analysis

For each of the different surface conditions, the measured WCAs ranged typically up to ± 10° around their mean values. This error is attributed firstly to the inhomogeneity in surface topography and secondly to the possible variation in droplet sizes which was adjusted manually for each measurement and the goniometer error [34].

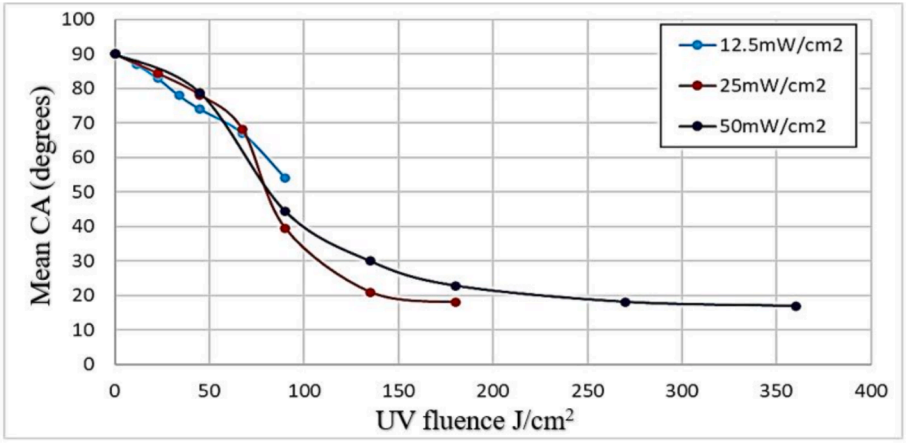

Fig. 9. Mean WCAs for CFRP samples treated with different UV fluence.

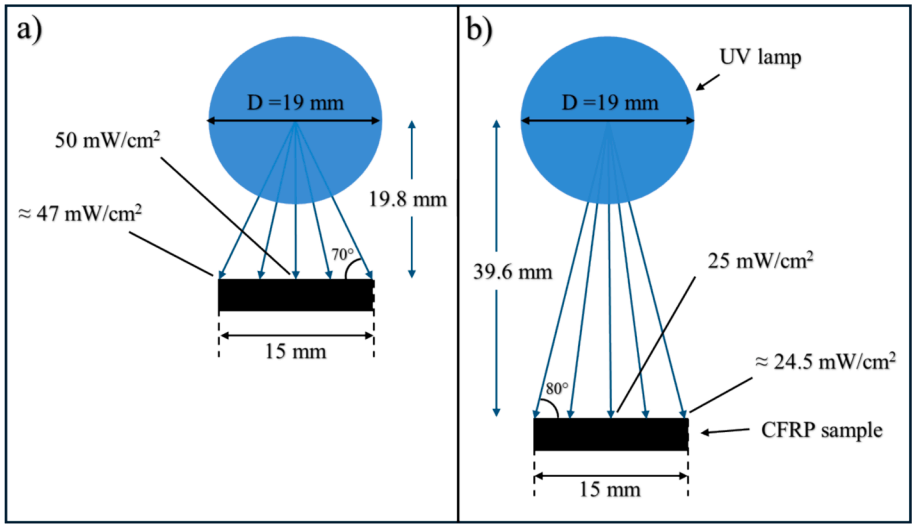

Fig. 10. Schemes show the UV intensity distribution over the width of samples exposed to a) 50 mW/cm^2, and b) 25 mW/cm^2.

UV treatment generally improved the wettability of the CFRP surfaces. WCAs (Fig. 7) have significantly been reduced from hydrophobic into near super hydrophilic as higher UV fluences were used. Fig. 8 shows the reduction in mean WCA upon the different UV intensities and exposure periods, Fig. 9 shows that with the different UV intensities used, the reduction in WCA was based on the UV fluence, in other words, the higher the UV intensity used, the less time needed to reduce the WCA.

In Figs. 8 and 9, which illustrate the relationship between WCA and UV exposure and fluence, there appears to be an initial linear change followed by a non-linear variation. The mean WCA initially decreases slightly from 90° to around 70° or 80° within the first 50 J/cm^2, then significantly lowers to around 30° or 40° with the next 50 J/cm^2 of UV fluence, with minimal further reduction afterwards. At 200 J/cm^2, the mean WCA is around or just under 20°. Similar non-linear behaviour of WCA versus UV exposure has been reported in the literature for some polyimide films [35]. This occurs because UV light at 254 nm interacts with polymeric molecules by breaking molecular bonds whose binding energy is less than its photon energy (4.88 eV). This interaction leads to chain scission accompanied by the formation of unsaturated products in the polymer chains and the creation of free radicals on the polymer surface. These radicals can react with oxygen in the air to form carboxyl and hydroxyl groups. The formation of unsaturated groups and the presence of carboxyl and hydroxyl groups increase the absorbance of the polymeric material upon UV-C irradiation. The increase in absorbance with increasing UV exposure can explain the non-linear (rapid) reduction in WCA [36]. Additionally, it is noticed from Fig. 9 that above 80 J/cm^2 the contact angle at 25 mW/cm^2 exposure drops below that at 50 mW/cm^2. This can be attributed to multiple reasons. Firstly, the effect of the exposure period: although the same UV fluences are used, longer exposure times might provide more opportunity for the already generated free radicals to react with oxygen. This results in an increased formation of oxidative products over time, which in turn increases the absorbance, as described earlier. However, a review of the literature does not clearly confirm this relationship.

The more likely reason, however, can be attributed to the distances between the samples and the cylindrical UV lamp. The closer the distance between the lamp and the sample, the less uniform the distribution of UV intensity over the sample surface, with the intensity decreasing towards the sample edges (see the scheme in Fig. 10). Additionally, the light incident angle at the edges of the samples, which likely influences the reflection, corresponds to the two intensities being approximately 70° and 80°, respectively. Note that for accuracy, the measurements of the CAs were mostly performed close to the edges of the samples.

The WCA measurements reported in Figs. 8 and 9 belonged to UV-treated and non-treated samples were based on the final stable state of the test droplet. In laser-textured samples, the WCA continued to decrease, this is due to the continual spreading of the water droplet

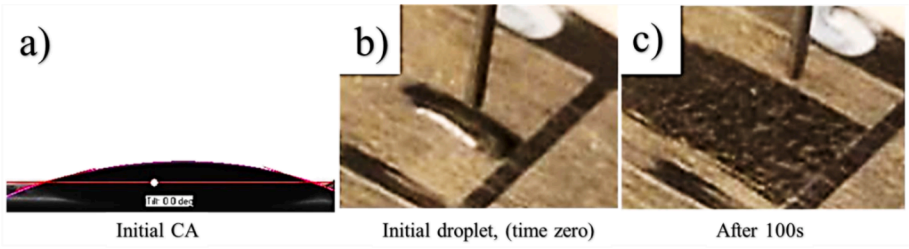

Fig. 11. A) an initial wca for laser treated sample, and photos of the droplet to clarify the absorption behaviour of the fibre exposed cfrp and the time dependency of the ca b) at time zero and c) at time 100 s.

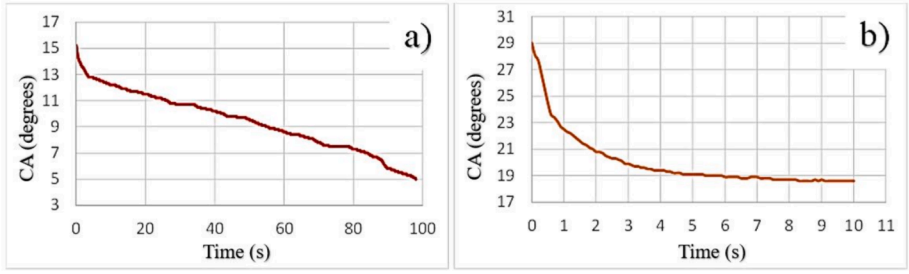

Fig. 12. Typical time dependency for the reduction or stability of WCA of, a) laser textured, b) UV treated sample.

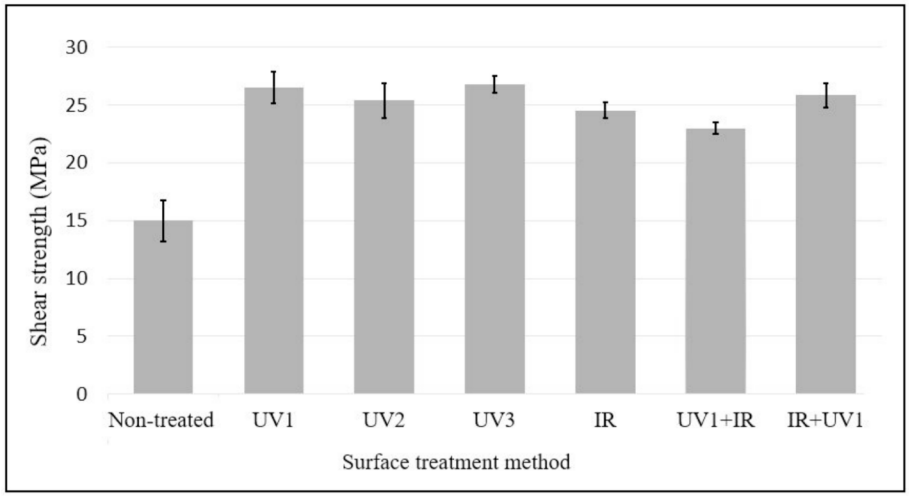

Fig. 13. Comparison of the bonding strength via SLS tests among different surface conditions. For combined, UV1 + IR indicates that the UV treatment was applied first, and the same applies to IR+UV1.

across the sample, indicating its penetration through the laser-textured CFRP surface (Fig. 11). The initial average WCA for laser-textured samples was about 15° and dropped to under 5° within 100 s. In contrast, for samples that were treated with the highest UV fluence, the initial average WCA was around 30° and stabilised at around 20° in less than 5 s.

The graphs in Fig. 12 illustrate examples of the time dependency of WCA reduction for a laser-textured sample and a UV-treated sample. With regards to the WCA of laser-textured material, the current findings are in line with other researchers who investigated the absorption nature of porous materials [34].

For both combined treatment techniques (UV+IR and IR+UV), the wettability results were similar to those obtained with IR laser treatment alone. It was challenging to detect any significant variations between samples due to the contact angle dropping close to 0°.

3.3. Single Lap shear (SLS) tests

In comparison with non-treated samples, results from SLS tests (Fig. 13) show significant (70–80 %) improvement in the bonding strength for all treatment techniques.

Samples treated with UV light revealed better strength than those treated with IR laser solely or in combination with UV light. The average bonding strength was about 27 MPa for UV1 and UV3 and was just above 25 MPa for UV2. Samples textured with IR laser only showed an average bonding strength of less than 25 MPa. Pre-treatment with UV prior to laser texturing shows a slight reduction in the bonding strength while the bonding strength improved when the UV treatment followed the laser texturing. For the combined treatments, such slight variations cannot be considered statistically significant due to the limited number of repeated samples. The failure modes for the UV-treated samples were completely different than those treated with laser solely or in

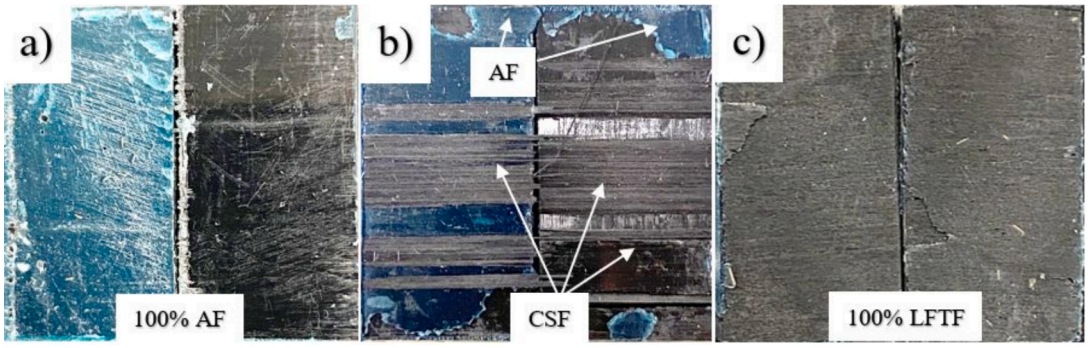

Fig. 14. The failure modes of, a) non-treated sample, b) UV treated, c) laser treated.

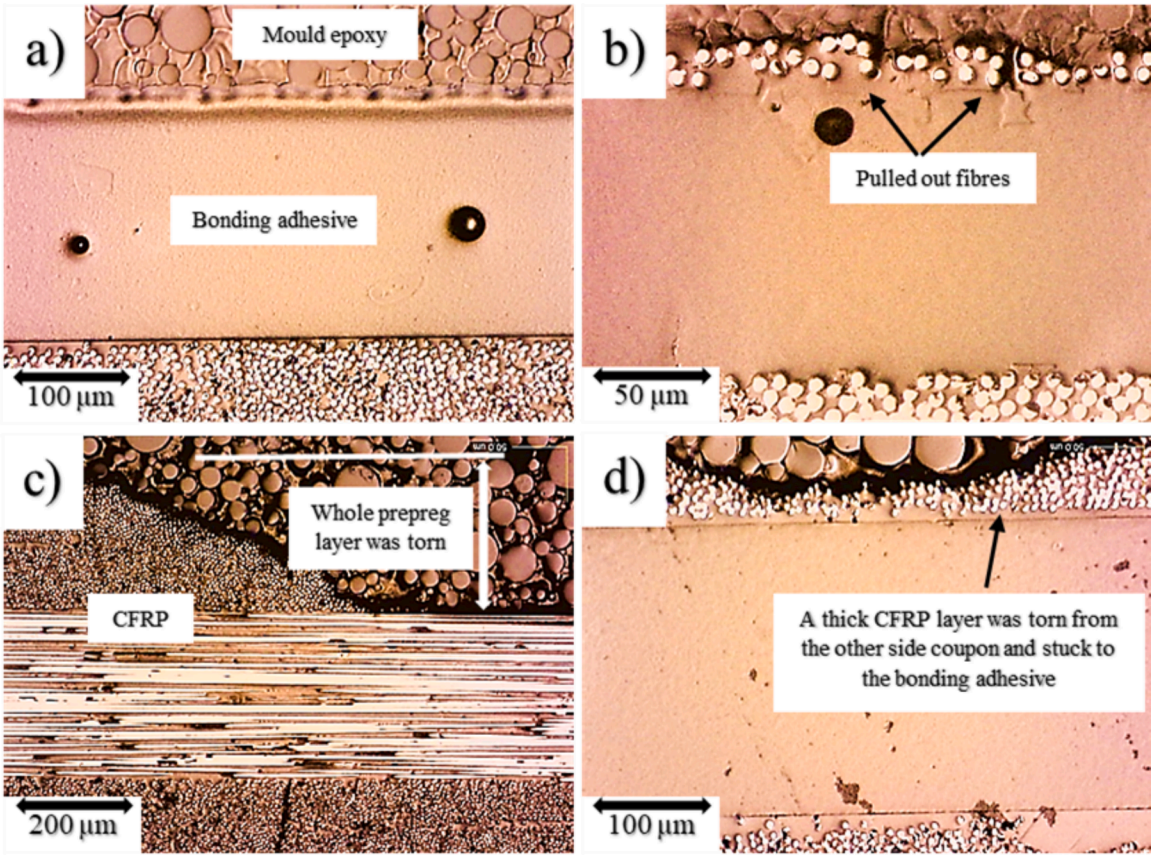

Fig. 15. Fracture analysis using optical microscopy, CFRP cross-section after SLS test, a) non-treated sample covered with bonding adhesive, b) laser-treated sample covered with bonding adhesive with pulled out fibres detected on top of the adhesive, c) UV treated sample with thick layer torn out from it, d) UV treated sample covered with adhesive and thick torn out layer detected on top of the adhesive.

combination with UV light. Fig. 14 shows the three different failure modes. The failure modes are categorized according to the classification system provided by Banea and Silva [37].

In addition to the macro photos of the failure modes in Fig. 14 and for further clarification, fracture analysis optical microscopy of the cross-section of the failed samples was conducted (Fig. 15). Non-treated samples have exhibited 100 % Adhesive Failure (AF) where the failure occurs at the adherend/adhesive interface (Fig. 15a). This was expected due to the low adhesion strength between the bonding adhesive and the non-treated substrate material. For the three laser techniques (including the combined treatment), the failure was 100 % Light Fibre Tear Failure (LFTF). The optical microscopy image of the cross-section (Fig. 15b) showed up to three layers of fibre were pulled out from one side and stuck to the bonding adhesive on the other side. This is because IR laser texturing possibly weakened the bonding between the CFs at the surface and the matrix resin. This observation is in line with some previous studies [12,38]. These stated that after IR laser treatment, cavities were detected near the surface between the exposed fibres and the matrix.

Unlike the laser-treated samples, the failure modes for UV-treated samples were a mix of mostly Cohesive Substrate Failure (CSF) and to a lesser extent AF. Optical microscopy images (Fig. 15b) show up to 0.25 mm thick torn layer from the substrate. The CSF happened mostly at or near the interface between the first and second prepreg layers and was not only within the bonded region but along the whole coupon in some samples, Fig. 16.

The cross-section assessment (Fig. 15) reveals small bubbles within the adhesive layer of some samples, believed to have formed during the mixing of the bonding adhesive. Since the failure of all samples did not

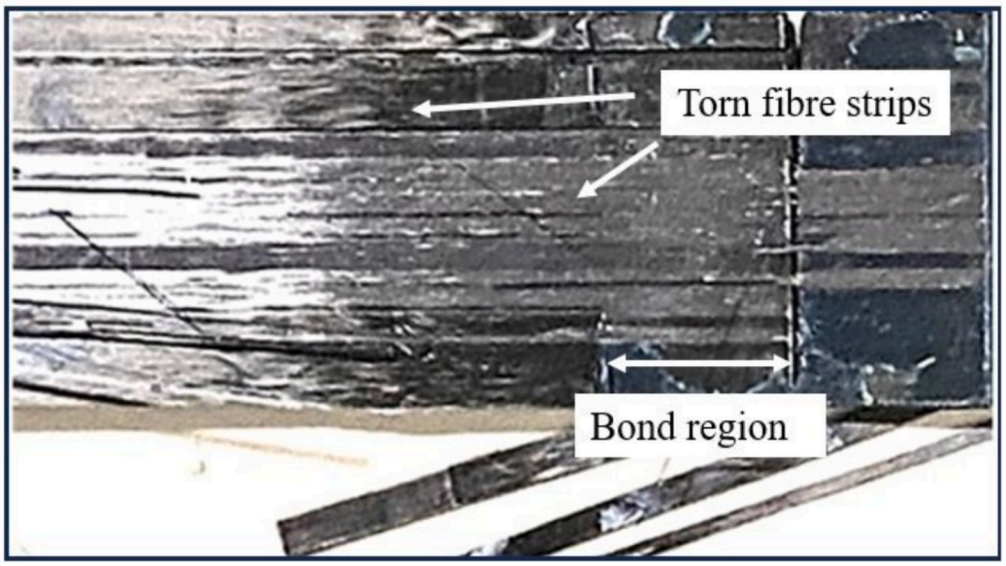

Fig. 16. Macro photo showing fractured UV treated sample, the fracture is along the entire coupon.

occur within the adhesive layer, it is presumed that these small bubbles had no significant impact on the recorded bonding strength.

The CSF can be attributed to several factors. Firstly, the layup orientation and sequence play a significant role in determining the eccentricity of the load path and, consequently, the peeling forces [37,39]. Secondly, fibre reinforced polymer composites generally have low through-thickness strength, accordingly, high strength adhesive joints are more likely to fail within the composite due to peeling stresses before failure in the adhesive occurs [37,40]. Although UV treatment shows slight improvement (about 10 %) over laser texturing, the predominant occurrence of CSF, mainly at the interface between the first and second prepreg layers of the UV treated samples, suggests that the tested CFRP material has nearly reached its maximum bonding strength for the utilized joint design. Therefore, it is hypothesized that utilizing stronger CFRP material may yield further advancement for the UV treatment.

4. Conclusions

In this work, CFRP material manufactured with five layers of unidirectional carbon fibre prepreg was surface treated using different techniques, UV light, IR laser, and IR laser combined with UV light. The wettability and the adhesive bonding strength of the treated surfaces were qualitatively characterised. The following conclusions were obtained:

- The UV light treatment technique for CFRP demonstrated a significant (75 %) improvement in bonding strength compared to non-treated samples, and approximately 10 % higher improvement than the IR laser texturing technique. The dominant Cohesive Substrate Failure (CSF) mode observed in UV-treated samples suggests that the adhesion strength exceeded the material's interlaminar shear strength.
- Both UV light and IR laser treatments significantly improved the wettability of the CFRP surface. The water contact angle reduced from 90° to approximately 20° for UV treatment and to under 10° for IR laser treatment. However, the absorption behaviour of the exposed fibre surfaces (IR laser treated) has a contribution.
- The combination treatments do not appear to provide any noticeable advantage over the individual treatments.
- The laser processing period for a single coupon which has a bonded area of 25 mm x 12.5 mm was approximately 11 s, while the UV treatment took one hour. However, with UV treatment, multiple samples (over 100) can be treated simultaneously. Furthermore, the processing time with UV light can be reduced by using certain reflectors, such as semi-cylindrical or parabolic reflectors, to increase the intensity. More uniformly distributed light can also be achieved by using a diffuser.
- The results from the UV treatment are highly promising, suggesting significant potential for enhancing the joint performance of CFRP composites by enhancing adhesive bonding without altering the surface topography.

CRediT authorship contribution statement

Ahmed Al-Mahdy: Writing – original draft, Visualization, Validation, Methodology, Investigation, Data curation. **Juan Ignacio Ahuir-Torres:** Writing – review & editing, Supervision, Investigation. **Tahsin Tecelli Öpöz:** Writing – review & editing, Supervision, Investigation. **Hiren R Kotadia:** Writing – review & editing, Supervision, Investigation. **Jack Mullett:** Writing – review & editing, Supervision, Investigation. **Martin Charles Sharp:** Writing – review & editing, Supervision, Project administration, Methodology, Investigation, Conceptualization.

Declaration of competing interest

The authors declare that they have no known competing financial interests or personal relationships that could have appeared to influence the work reported in this paper.

Data availability

Data will be made available on request.

Acknowledgment

The authors would like to express their gratitude to the technicians at Liverpool John Moores University, particularly Mr. Harvey Thompson, for their assistance in conducting the mechanical tests.

References

[1] S. Li, T. Sun, C. Liu, W. Yang, Q. Tang, A study of laser surface treatment in bonded repair of composite aircraft structures, R. Soc. Open Sci. 5 (3) (2018) 171272.

[2] V. Oliveira, S. Sharma, M. De Moura, R. Moreira, R. Vilar, Surface treatment of CFRP composites using femtosecond laser radiation, Opt. Lasers Eng. 94 (2017) 37–43.
[3] R. Teti, T. Segreto, A. Caggiano, L. Nele, Smart multi-sensor monitoring in drilling of CFRP/CFRP composite material stacks for aerospace assembly applications, Appl. Sci. 10 (3) (2020) 758.
[4] T.L. See, Z. Liu, S. Cheetham, S. Dilworth, L. Li, Laser abrading of carbon fibre reinforced composite for improving paint adhesion, Appl. Phys. A 117 (2014) 1045–1054.
[5] A. Baldan, Adhesion phenomena in bonded joints, Int. J. Adhes. Adhes. 38 (2012) 95–116.
[6] S. Ebnesajjad, C. Ebnesajjad, Surface treatment of materials for adhesive bonding, William Andrew, 2013.
[7] F. Fischer, S. Kreling, P. Jäschke, M. Frauenhofer, D. Kracht, K. Dilger, Laser surface pre-treatment of CFRP for adhesive bonding in consideration of the absorption behaviour, J. Adhes. 88 (4–6) (2012) 350–363.
[8] D. Wang, Y. Li, T. Zou, J. Fu, Z. Liu, Increasing strength and fracture toughness of carbon fibre-reinforced plastic adhesively bonded joints by combining peel-ply and oxygen plasma treatments, Appl. Surf. Sci. 612 (2023) 155768.
[9] M. Kanerva, O. Saarela, The peel ply surface treatment for adhesive bonding of composites: A review, Int. J. Adhes. Adhes. 43 (2013) 60–69.
[10] J. Holtmannspötter, J. Czarnecki, M. Wetzel, D. Dolderer, C. Eisenschink, The use of peel ply as a method to create reproduceable but contaminated surfaces for structural adhesive bonding of carbon fiber reinforced plastics, J. Adhes. 89 (2) (2013) 96–110.
[11] P.W. French, A. Wolynski, M. Naeem, M.C. Sharp, New Laser Machine Tools for Processing Carbon Fibre Reinforced Plastic (CFRP), Key Eng. Mater. 496 (2012) 30–35.
[12] V. Reitz, D. Meinhard, S. Ruck, H. Riegel, V. Knoblauch, A comparison of IR-and UV-laser pretreatment to increase the bonding strength of adhesively joined aluminum/CFRP components, Compos. A Appl. Sci. Manuf. 96 (2017) 18–27.
[13] C. Leone, S. Genna, Effects of surface laser treatment on direct co-bonding strength of CFRP laminates, Compos. Struct. 194 (2018) 240–251.
[14] P.A. Askeland, H. Fukushima, M. Rich, L.T. Drzal, UV Ozone Surface Modification of Carbon Based Reinforcements for Composite Materials, in: Composite Materials and Structures Center, Michigan State University:, East Lansing, MI, USA, 2004, p. 9.
[15] M. Rich, L. Drzal, B. Rook, P. Askeland, and E. Drown, "Novel carbon fiber surface treatment with ultravilet light in ozone to promote composite mechanical properties," in Proceedings of ICCM-17th conference, Edinburgh, 2009.
[16] T. Kamae, L.T. Drzal, Mechanical and thermal properties of high volume-fraction carbon nanotube/epoxy composites, and property enhancement by UV ozone treatment of carbon nanotubes, Polym. Compos. 44 (11) (2023) 7855–7864.
[17] M. Rich, E. Drown, P. Askeland, L. Drzal, Surface treatment of carbon fibers by ultraviolet light+ ozone: its effect on fiber surface area and topography, in: In the 19th International Conference on Composite Materials, 2013, pp. 1196–1204.
[18] S. Kawasaki, Y. Ishida, T. Ogasawara, Effect of vacuum–ultraviolet irradiation in a nitrogen gas atmosphere on the adhesive bonding of carbon-fiber-reinforced polyphenylene sulfide composites, J. Adhes. 98 (1) (2022) 90–104.
[19] E. Arikan, J. Holtmannspötter, F. Zimmer, T. Hofmann, H.-J. Gudladt, The role of chemical surface modification for structural adhesive bonding on polymers-Washability of chemical functionalization without reducing adhesion, Int. J. Adhes. Adhes. 95 (2019) 102409.
[20] M. Hamdi, M.N. Saleh, J.A. Poulis, Improving the adhesion strength of polymers: effect of surface treatments, J. Adhes. Sci. Technol. 34 (17) (2020) 1853–1870.
[21] J.R. Vig, UV/ozone cleaning of surfaces, J. Vac. Sci. Technol. A 3 (3) (1985) 1027–1034.
[22] M.D. Romero-Sánchez, M.M. Pastor-Blas, J.M. Martín-Martínez, M. Walzak, Addition of ozone in the UV radiation treatment of a synthetic styrene-butadiene-styrene (SBS) rubber, Int. J. Adhes. Adhes. 25 (4) (2005) 358–370.
[23] S.K. Øiseth, A. Krozer, J. Lausmaa, B. Kasemo, Ultraviolet light treatment of thin high-density polyethylene films monitored with a quartz crystal microbalance, J. Appl. Polym. Sci. 92 (5) (2004) 2833–2839.
[24] N. Nagai, T. Matsunobe, T. Imai, Infrared analysis of depth profiles in UV-photochemical degradation of polymers, Polym. Degrad. Stab. 88 (2) (2005) 224–233.
[25] J. Singh, IIT JEE Physics (1978 to 2018: 41 Years) Topic-wise Complete Solutions, 3rd ed., Telangana, India, 2018.
[26] D. Jiang, A.S. Alsagri, M. Akbari, M. Afrand, A.A. Alrobaian, Numerical and experimental studies on the effect of varied beam diameter, average power and pulse energy in Nd: YAG laser welding of Ti6Al4V, Infrared Phys. Technol. 101 (2019) 180–188.
[27] K.L. Wlodarczyk, et al., Laser microsculpting for the generation of robust diffractive security markings on the surface of metals, J. Mater. Process. Technol. 222 (2015) 206–218.
[28] D. Sola, A. Conde, I. García, E. Gracia-Escosa, J.J. De Damborenea, J.I. Peña, Microstructural and wear behavior characterization of porous layers produced by pulsed laser irradiation in glass-ceramics substrates, Materials 6 (9) (2013) 3963–3977.
[29] CEN. "British Standards Institute, BS EN 1465:2009 "Adhesives. Determination of tensile lap-shear strength of bonded assemblies", 2009, London, BSI.
[30] M. Schweizer, D. Meinhard, S. Ruck, H. Riegel, V. Knoblauch, Adhesive bonding of CFRP: a comparison of different surface pre-treatment strategies and their effect on the bonding shear strength, J. Adhes. Sci. Technol. 31 (23) (2017) 2581–2591.
[31] B. Duncan, "Developments in testing adhesive joints," in Advances in structural adhesive bonding, Elsevier (2010) 389–436.
[32] G. Zheng, C. Liu, X. Han, W. Li, Effect of spew fillet on adhesively bonded single lap joints with CFRP and aluminum-alloy immersed in distilled water, Int. J. Adhes. Adhes. 99 (2020) 102590.
[33] T. Bregar, et al., Carbon nanotube embedded adhesives for real-time monitoring of adhesion failure in high performance adhesively bonded joints, Sci. Rep. 10 (1) (2020) 1–20.
[34] S. Krainer, U. Hirn, Contact angle measurement on porous substrates: Effect of liquid absorption and drop size, Colloids Surf A Physicochem Eng Asp 619 (2021) 126503.
[35] Y. Tsuda, Surface wettability controllable polyimides by UV light irradiation for printed electronics, J. Photopolym. Sci. Technol. 29 (3) (2016) 383–390.
[36] M. Akkamma, B. Lobo, Optical properties of UV-C irradiated polyvinylidene chloride films, Radiat. Phys. Chem. 212 (2023) 111182.
[37] M.D. Banea, L.F. da Silva, Adhesively bonded joints in composite materials: an overview, Proceedings of the Institution of Mechanical Engineers, Part L: Journal of Materials: Design and Applications 223 (1) (2009) 1–18.
[38] S. Harder, H. Schmutzler, P. Hergoss, J. Holtmannspötter, B. Fiedler, Effect of infrared laser surface treatment on the morphology and adhesive properties of scarfed CFRP surfaces, Compos. A Appl. Sci. Manuf. 121 (2019) 299–307.
[39] S. Purimpat, R. Jérôme, A. Shahram, Effect of fiber angle orientation on a laminated composite single-lap adhesive joint, Adv. Compos. Mater 22 (3) (2013) 139–149.
[40] R.D. Adams, Strength predictions for lap joints, especially with composite adherends. A review, J. Adhes. 30 (1–4) (1989) 219–242.